

<https://doi.org/10.1038/s42004-024-01265-5>

Pressure induced structural and electronic band transition in CsPbBr₃

Check for updates

Dongzhou Zhang^{1,7,8}✉, Sagarmoy Mandal^{2,7}, Duck Young Chung³, Jingui Xu⁴, Nannan Shan⁵,
Mercouri G. Kanatzidis^{3,6} & Ming Chen^{2,8}✉

Cesium lead bromide (CsPbBr₃) is a prominent halide perovskite with extensive optoelectronic applications. In this study, we report the pressure modulation of CsPbBr₃'s crystal structure and electronic properties at room temperature up to 5 GPa. We have observed a crystal structure transition from the orthorhombic Pnma space group to a new monoclinic phase in the space group P2₁/c at 2.08 GPa. The structure is associated with ~8% of density jump across the transition boundary. DFT calculations have suggested that the structure transition leads to a change in the electronic band structure, and there is an emergent indirect bandgap at the Pnma-P2₁/c phase transition boundary at 2.08 GPa. Across the transition boundary, the electronic band gap of CsPbBr₃ increased from 2.07 eV to 2.38 eV, which explains its pressure-induced color change. Our study demonstrates the importance of using in-situ crystal structure in the electronic band structure calculations in halide perovskites.

In recent years, the perovskite-structured CsPbBr₃ has attracted researchers' attention because of its impressive optoelectronic properties. CsPbBr₃ has long carrier life, high electron mobility, and decent thermal stability, making it a great candidate for photovoltaics applications¹. Most prominently, CsPbBr₃ has demonstrated a photoluminescence quantum yield (PLQY) of >95%, nonparallel by any other halide perovskites^{1,2}. The high PLQY of CsPbBr₃ not only makes it an efficient base material for radiation detection^{3,4}, but also gives it the potential in photoluminescence display devices^{5,6}. Because of these characteristics, CsPbBr₃ is an emerging candidate material in many optoelectronic applications.

Pressure has been observed to have a strong effect on the optoelectronic properties of CsPbBr₃. Gong et al. has observed that the PLQY of bulk CsPbBr₃ crystal peaks at ~1.2 GPa, more than 90 times of its room pressure value². Pressure is also known to affect the bandgap of CsPbBr₃. At pressures below 1 GPa, the bandgap is suppressed with pressure^{2,7,8}, whereas at pressures higher than 1 GPa, both density functional theory (DFT) calculation and photoluminescence (PL) experiments have confirmed that the bandgap increases with pressure^{2,7,8}. The mechanism behind this bandgap change is the pressure-induced structural transition in CsPbBr₃. It has been observed that CsPbBr₃ preserves its Pnma perovskite structure till 1.5–2.5 GPa, yet there is no consensus on the crystal structure of CsPbBr₃ crystal

at pressures above 2 GPa. One powder diffraction experiment has suggested that CsPbBr₃ becomes amorphous at pressures above 2 GPa⁸, while DFT calculations have suggested that CsPbBr₃ either maintains the Pnma space group at high pressures but have a different structure², or transforms into a P2₁2₁2₁ polar structure⁷. In either case, the high-pressure phase is believed to have an indirect bandgap^{2,7,8}. Because of the high-pressure crystal structure of CsPbBr₃ strongly modulates its electronic bandgap, it is imperative to carry out a careful crystallographic measurement on CsPbBr₃ crystals at high pressures.

Single crystal X-ray diffraction (SXRD) has proven a useful tool to accurately constrain the structure of halide perovskites at high pressures⁹. Using large-opening diamond anvil cells and SXRD, multiple structural transitions in halide perovskites have been identified between 0.5 and 15 GPa^{10–14}, and most of these structural transitions are displacive phase transitions¹⁵ that involve space group change. In this paper, we report our measurement on the high pressure phase transition of CsPbBr₃ using high pressure SXRD. We have identified a phase transition from Pnma orthorhombic space group to P2₁/c monoclinic space group at 2 GPa. DFT calculations have shown an electron bandgap change associated with the phase transition similar to previous reports. Our results provide new insights into the pressure-modulation of the optoelectronic properties in halide perovskite.

¹GeoSoilEnviroCARS, University of Chicago, Argonne, IL, USA. ²Department of Chemistry, Purdue University, West Lafayette, IN, USA. ³Materials Science Division, Argonne National Laboratory, Argonne, IL, USA. ⁴Institute of Geochemistry, Chinese Academy of Sciences, Guiyang, Guizhou, China. ⁵Research Computing at Purdue University, West Lafayette, IN, USA. ⁶Department of Chemistry, Northwestern University, Evanston, IL, USA. ⁷These authors contributed equally: Dongzhou Zhang, Sagarmoy Mandal. ⁸These authors jointly supervised this work: Dongzhou Zhang, Ming Chen. ✉e-mail: dzzhang@cars.uchicago.edu; chen4116@purdue.edu

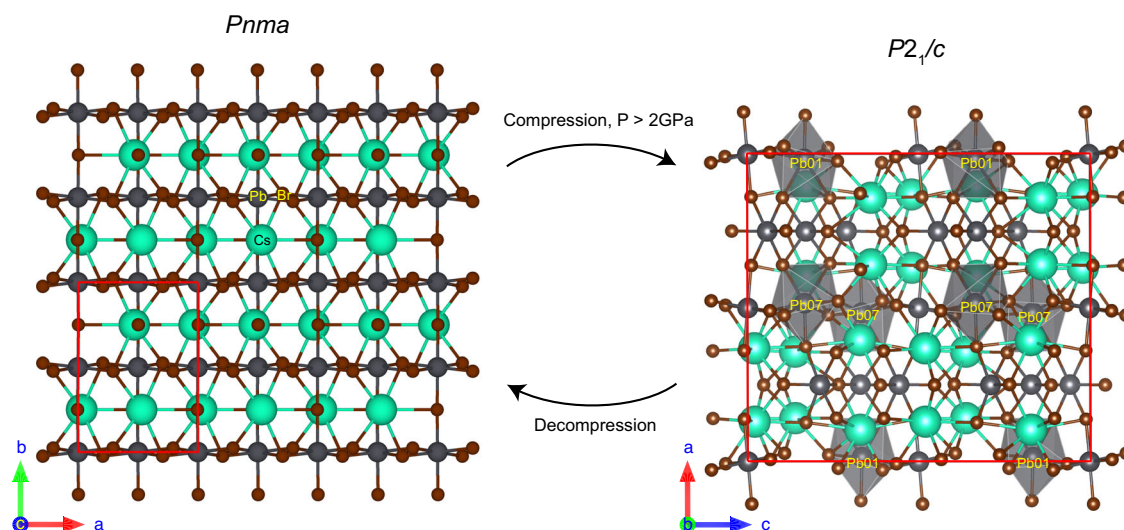


Fig. 1 | Single crystal structures of the low-pressure (left) and high-pressure (right) phases of CsPbBr₃. The red boundaries indicate the unit-cell of each phase. 7-coordinated Pb sites (Pb01 and Pb07) in the high pressure phase are highlighted with the grey polyhedra.

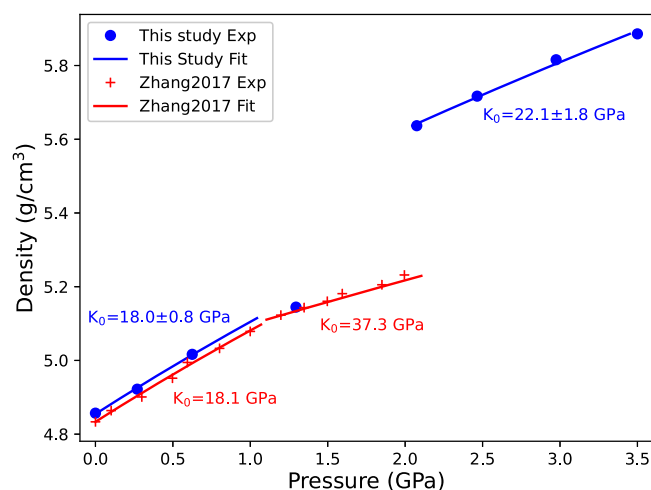


Fig. 2 | Density of CsPbBr₃ as a function of pressure. Curves in the figure indicate the best-fit BM2-EoS, with the best-fit bulk modulus K_0 labeled next to each EoS.

Results and discussions

High pressure crystal structure of CsPbBr₃

From high pressure SXD data, we found that the CsPbBr₃ crystal underwent a phase transition from orthorhombic structure (space group Pnma, #62) to a more distorted monoclinic structure (space group P2₁/c, #14) at 2 GPa (Fig. 1). In this process, the unit cell expands to include six times more atoms whereas the density of the crystal increased by ~8% from 5.23 g/cm³ to 5.64 g/cm³ (Fig. 2). We have observed that for the high pressure P2₁/c phase, two of the Pb sites (Pb01 and Pb07) changes from 6-coordinated to 7-coordinated (Fig. 1). Although the β angle of the high pressure P2₁/c phase is very close to 90° (90.110–90.134°), in the structure we can't find either three perpendicular 2-fold axes, or one 2-fold axis and two mirror planes. We have also attempted to solve the crystal structure with an orthorhombic starting model, yet the structure solution/refinement didn't converge, so we conclude that the crystal system of the high pressure phase has to be monoclinic.

We also determined the density and equations of states of the low pressure and high pressure phases of CsPbBr₃ and compared them with published data. At pressures below 2 GPa, our results is consistent with

published powder diffraction measurements⁸. It has been suggested that the Pnma structured CsPbBr₃ will undergo an isostructural transition at 1.2 GPa⁸, in which the crystal maintains the same space group but the bulk modulus K_0 increases from 18.1 GPa to 37.3 GPa when fitting the P-V data with a second-order Birch-Murnaghan equation of states (BM2-EoS):

$$P(V) = \frac{3K_0}{2} \left[\left(\frac{V_0}{V} \right)^{7/3} - \left(\frac{V_0}{V} \right)^{5/3} \right],$$

where V_0 is the unit cell volume at 0 GPa. Our data show the same kink in pressure-density relationship below and above 1.2 GPa (Fig. 2). When fitting our measured P-V data below 1.2 GPa (usually referred to as the phase-I, and phase-II refers to the structure between 1.2 and 2 GPa^{2,8}) with BM2-EoS, the best-fit bulk modulus K_0 of phase-I is 18.0 ± 0.8 GPa, consistent with powder X-ray diffraction results (18.1 GPa)⁸. The P-V relationship of the high pressure P2₁/c phase is also fitted with a BM2-EoS, and the best fit K_0 is 22.1 ± 1.8 GPa, which lies between the K_0 of phase-I and phase-II. The best-fit V_0 for the P2₁/c phase is 4437 ± 32 Å³. The V_0 for the Pnma phase is 793 ± 5 Å³. Considering that one unit cell in the P2₁/c phase corresponds to six unit cells in the Pnma phase, at zero pressure, the density of the Pnma phase is ~7% smaller than the P2₁/c phase.

We notice that, the bulk modulus K_0 for Pnma Phase-I (0–1 GPa) is 18.0 GPa, K_0 for Pnma phase-II (1–2 GPa) is 37.3 GPa, and K_0 for P2₁/c phase (>2 GPa) is 22.1 GPa. K_0 for Pnma phase-II is significantly higher than the other two. We suspect that this phenomenon indicates that the Pnma-P2₁/c transition has a martensitic-like nature. Martensitic transition¹⁶ involves rotation of polyhedra within the crystal structure, and has been observed in other perovskite-structured materials¹⁷. It is also known that pressure induced martensitic transition has significant effect on the bulk moduli of materials¹⁸, so we suspect that the abrupt change in the bulk moduli before and after the Pnma-P2₁/c transition indicates its martensitic-like nature.

Electronic band structure at high pressures

During our measurement, we monitor the evolution of sample color at various pressures. The sample starts as a brown colored translucent crystal. When the phase transition occurs at 2 GPa, the color of the crystal changes from brown to light yellow in back-reflection light (Fig. 3), which has been observed by multiple studies before^{2,8,19}. The change of the sample color from brown to transparent is an indicator that the sample no longer absorbs green light near ~530 nm, which coincides with the observations from optical absorption spectroscopy^{2,8,20}. On release of the pressure after

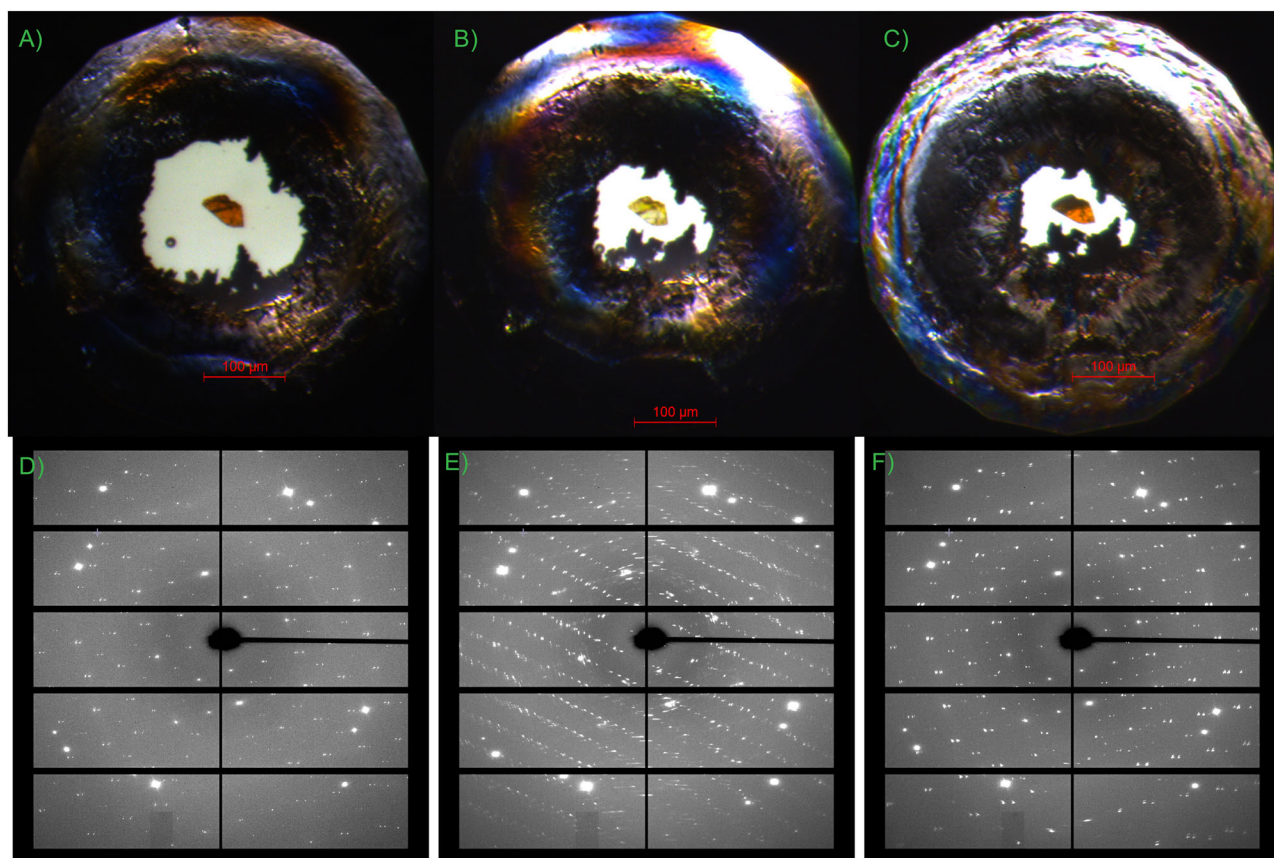


Fig. 3 | Optical images (top) and corresponding merged diffraction images (bottom) of CsPbBr₃ at various pressures. Sample is located at the center of the Regasket hole and a small piece of ruby sphere is located close to the sample as pressure

marker. A&D): 0.27 GPa (right after gas loading). B&E): 2.08 GPa (right after the structural transition). C&F): 1 bar after decompression.

decompression, the sample's color changes back to brown, and the diffraction images switched back to the Pnma diffraction pattern as well (Fig. 3), showing that the pressure-induced Pnma-P2₁/c transition is reversible.

The change of sample's color is strongly related to the electronic band structure evolution in the sample. In order to examine the association of the electronic band structure as a function of pressure, we have carried out DFT calculations based on the high pressure crystal structure we resolved with SXD (Fig. 4). Below the structural transition pressure at 2 GPa, the band gap of the low pressure Pnma phase gradually decreases from 2.09 eV at 1 bar to a minimum of 2.05 eV at 1.5 GPa, then increases to 2.07 eV at 2 GPa, and the same pressure dependence of band gap has been observed in multiple experimental^{2,8,20} and DFT^{2,7,8,21} studies before. This non-monotonic pressure dependence of the band gap has been interpreted as the result of competition between isotropic volume deformation and structural relaxation²².

After the Pnma-P2₁/c structural transition, our calculations have demonstrated that the valence band maximum shifted from Γ -point (0, 0, 0) to around Z-point (0, 0.5, 0) (Fig. 4C), whereas the conduction band minimum stays at the Γ -point (Fig. 4B), which indicates the emergence of an indirect bandgap in the high pressure P2₁/c phase, consistent with experimental observations². Our calculations also show that the high pressure phase has a bigger band gap than the low pressure phase (Fig. 5). At the Pnma-P2₁/c transition, the band gap of CsPbBr₃ jumps from 2.07 eV to 2.38 eV, and similar band gap jumps have been experimentally observed across the 2 GPa phase transition boundary in both nano-crystalline²⁰ (0.25 eV) and single crystal² CsPbBr₃ (0.23 eV) (Fig. 5, inset). We note here that the experimental band gaps are measured using the Tauc method^{2,8,20}. High pressure optical absorption spectra were measured between 250 and

1100 nm. Experimental band gap was then calculated by extrapolating the linear part of $(adh\nu)^2-h\nu$ curve. The 0.31 eV band gap jump shifts the optical absorbance edge from ~540 nm to ~475 nm, and hence leads to the change in sample color from brown to light yellow (Fig. 3). The band gap of the high pressure P2₁/c phase also has a negative slope as a function of pressure, which is consistent with published experimental measurements on single crystal CsPbBr₃², where a negative band gap-pressure slope were observed between 5 and 40 GPa in a compression run, and between 1 and 30 GPa in a decompression run. At pressures above 3.5 GPa, we notice that the band gap of CsPbBr₃ becomes direct again (Fig. S1), which is similar to the predicted P2₁/m high pressure metastable phase². In conclusion, our DFT calculations have demonstrated that the Pnma-P2₁/c structural transition can explain the experimental optical measurements on CsPbBr₃ at high pressures. Our results highlights the necessity of using in-situ crystal structure in the calculation of electronic band structures of halide perovskites.

Our study also demonstrates the importance of pressure medium in high pressure DAC experiments. It has been pointed out by Szafranski and Katrusiak²³ and Zhang et al.²⁴ that the hydrostaticity of the pressure medium used in the DAC could control the kinetics and even the resultant phase of the pressure-induced phase transition. We notice that in the two experiments (G2020²⁰ and G2022²) that used silicone oil as the pressure medium, the bandgap jump right after the transition around 2 GPa was smaller (0.25 eV for G2020 and 0.23 eV for G2022) than our value (0.31 eV). Meanwhile, in both G2020²⁰ and G2022², the bandgap continues to increase over the range of 1–3 GPa by an additional 0.05 eV after the transition, and then decrease with pressure², yet in our study the bandgap decreases with pressure right after the Pnma-P2₁/c transition (Fig. 5). We suspect that this phenomenon indicates that the pressure-induced transition in CsPbBr₃ is slow in non-hydrostatic silicone oil pressure medium, and similar kinetics

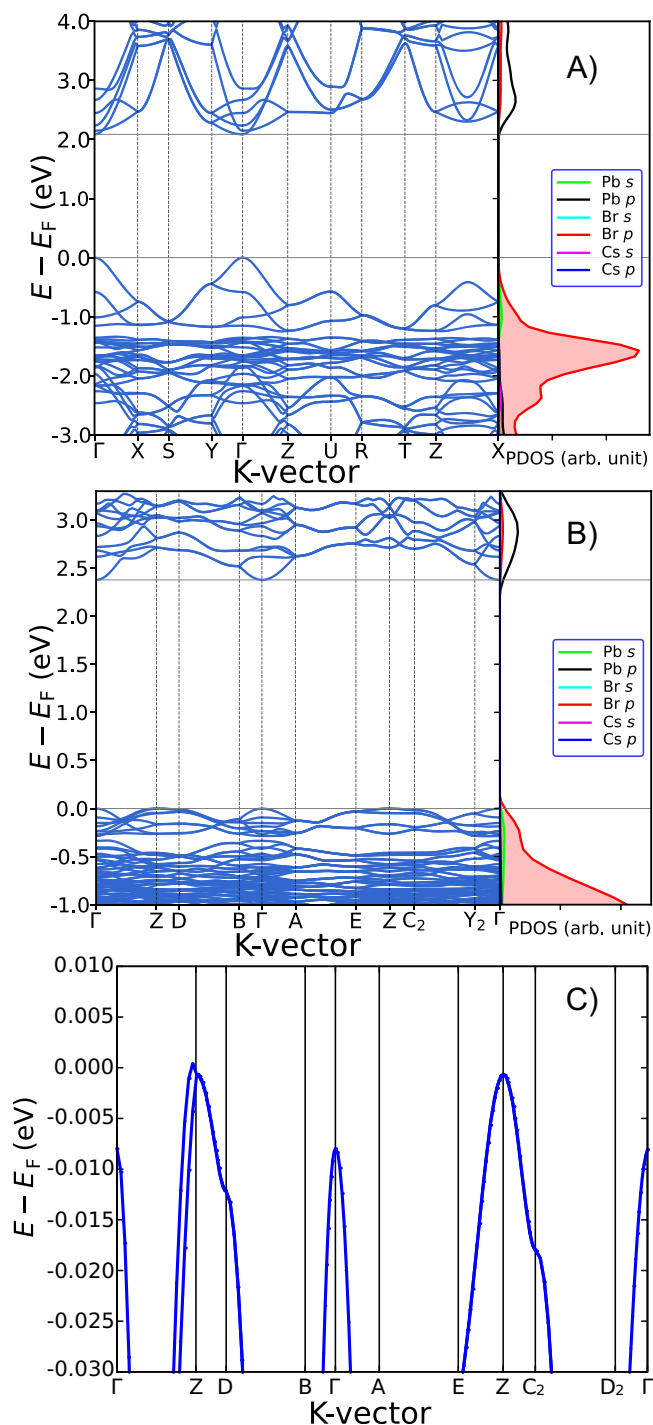


Fig. 4 | Electronic band structure and projected density of states (PDOS) of CsPbBr₃. Calculations at **A)** 1 bar (Pnma) and **B)** 2.08 GPa (P_{21/c}). **C** zoomed-in band structure at the top of valence band at 2.08 GPa, highlighting the high electronic energy near the Z-point (0, 0.5, 0). Since the bottom of the conduction band is around the Γ -point (0, 0, 0), we conclude that there is an emergent indirect bandgap in the P_{21/c} phase CsPbBr₃ at 2.08 GPa.

has been observed in MAPbCl₃ perovskite²³. The bandgap of MAPbCl₃ increased by 0.05 eV at the same pressure over 280 h²³, which is close to the offset between our reported value and G2020 (0.31 eV vs. 0.25 eV). In the meantime, for the compression and decompression runs in G2022², the bandgap of CsPbBr₃ is distinct at around 2 GPa (Fig. 5). In G2022, for the compression run, at \sim 2 GPa, the band gap was \sim 2.3 eV, while for the decompression run, at \sim 2 GPa, the band gap was \sim 3.1 eV. Besides,

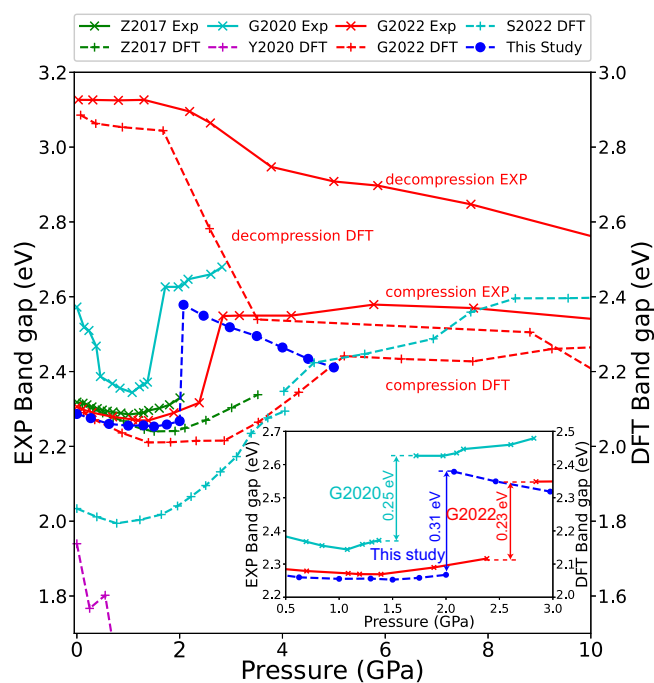


Fig. 5 | Experimentally determined and DFT computed electronic band gap of CsPbBr₃ as functions of pressure. Plus-signs and dashed curves: results from DFT calculations. Multiply-signs and solid curves: results from experimental measurements. Blue circles: band gap determined from this study using experimentally determined crystal structure as the initial structure for DFT calculations (Supplementary Table S1). Note the band gap from DFT (right axis) is shifted by 0.2 eV up relative to the band gap measured by experiments (left axis) to highlight the consistency between different studies, because DFT calculations tend to systematically underestimate the band gap³⁹. The value of 0.2 eV was chosen so that the experimental and DFT bandgaps in Gong et al.² and Zhang et al.⁸ at 1 bar would be aligned in the same figure. References: Z2017⁸, G2020²⁰, G2022², S2022⁷, Y2020²¹. Inset: Comparison between the band gap jump across the transition boundary in this study (blue) and two experimental measurements (red: G2022²; cyan: G2020²⁰).

the decompression run seems to have a discontinuity around the ambient pressure in G2022: the band gap dropped abruptly from \sim 3.1 eV at 0.03 GPa to 2.3 eV at 1 bar. We believe that this slow kinetics is a result of the non-hydrostatic pressure medium. On the other hand, we used neon pressure medium²⁵, which is hydrostatic up to 4.8 GPa. We conclude that the hydrostatic pressure environment is beneficial for a sharp phase transition boundary because of less deviatoric stress and pressure gradient²⁶.

Conclusions

We have studied the structural response of Pnma-structured CsPbBr₃ single crystal to high pressures using SXD and DAC. Similar to previous studies, we have observed a phase transition between 1.5 and 2.5 GPa. A careful structural solution and refinement using the SXD data suggests that the high pressure phase has a P_{21/c} space group, which hasn't been reported before. This structural transition is associated with \sim 8% density increase, and affects the mechanical properties such as the bulk modulus of CsPbBr₃.

Using DFT calculation, we have found that the Pnma-P_{21/c} transition is also associated with an electronic band gap jump of \sim 0.31 eV, which explains the sample's color change from brown to light yellow observed at high pressures. The structural transition also leads to the emergence of an indirect bandgap at 2.08 GPa, which has been substantiated experimentally. Besides, we predict another indirect to direct bandgap crossover at pressures above 3.5 GPa. We have demonstrated that most of the optical measurement results can be explained by the Pnma-P_{21/c} transition, and we expect our study on the pressure-induced phase transition in CsPbBr₃ will shed new insight into modulating the optoelectronic properties of halide perovskites with pressure.

Methods

Sample synthesis and crystal growth

CsPbBr₃ was synthesized by heating a stoichiometric mixture of CsBr and PbBr₂ sealed in a quartz tube under vacuum at 10⁻⁴ mbar at 650 °C overnight. Subsequently, a well-formed orange-colored CsPbBr₃ crystal was grown using the Bridgman method with a 3-zone furnace equipped with a translation unit. Growth conditions were maintained at temperatures of 450–600–300 °C and a growth speed of 1.0 mm/h. Pictures from the same batch of sample are shown in He et al.⁴

High pressure SXD measurement

A 50 μm × 30 μm × 10 μm fragment of CsPbBr₃ single crystal was loaded into a short symmetric DAC for high pressure SXD measurement²⁷. The DAC has a ±30° opening angle and the diamond culet diameter is 500 μm. A 0.25 mm thick Re gasket is used in the DAC and a ~200 μm diameter hole is drilled in the center of the gasket to serve as the sample chamber. Helium was used as the pressure medium²⁸ for the high-pressure SXD experiment, and ruby fluorescence was used to calibrate the pressure of the sample²⁹. The diffraction data were collected at the experimental station 13-BM-C of the Advanced Photon Source, Argonne National Laboratory²⁷. The X-ray beam was monochromated with silicon (311) crystal to 28.6 keV, with 1 eV bandwidth. A Kirkpatrick-Baez mirror system was used to obtain a vertical × horizontal focus spot size of 18 μm × 12 μm, measured as full width at half maximum. The Pilatus 3 S 1 M detector (Dectris) was placed about 200 mm away from the sample, and ambient NIST SRM660a LaB₆ powder was used to calibrate the distance and tilting of the detector. The CsPbBr₃ crystal was aligned to the rotation center of the diffractometer by absorption profile scan²⁷. A series of φ-exposures covered the full angular range of the DAC from φ = -30° to φ = 30°, and each image covers 1° width. The exposure time per frame was 1 s/φ. The diffraction images were reduced to peak intensity tables using APEX4 software package (Bruker), and the crystal structure was refined using the SHELX software package interfaced by Olex2^{30,31}. We have included Supplementary Fig. S3 to demonstrate the integrated diffraction pattern, the refined intensity profile and the residual for the high pressure P2₁/c phase at 2.08 GPa. Figures of merits for the structure refinement before and after the Pnma-P2₁/c transition are listed in Supplementary Table S3.

DFT calculations

DFT calculations were carried out using Quantum ESPRESSO software package^{32,33} to compute the structural and electronic properties. Initial structure from the SXD measurements at each pressure was used as the input for crystal structure relaxation in plane-wave self-consistent field calculation. Perdew–Burke–Ernzerhof (PBE)³⁴ functional was used together with the projector augmented wave (PAW)³⁵ type of pseudopotentials. The PAW pseudopotentials are used because they offer an optimal balance between accuracy and computational cost and^{36,37} have been successfully used in previous studies to predict properties similar to those investigated in our work^{36,38}. The convergence threshold on total energy, maximum force and pressure were set to 2 × 10⁻⁴ Ry, 4 × 10⁻⁴ Ry/a.u., and 0.05 GPa, respectively. The energy cutoff for wave functions was set to 80 Ryd, and the energy cutoff for charge density and potential was set to 400 Ryd. The Brillouin zone was sampled with Γ-centered k-point mesh of 4 × 3 × 4 and 1 × 3 × 1 for the orthorhombic and monoclinic systems, respectively. The experimental and computed crystal structures are compared in Supplementary Table S2 and Figure S4. The k-point meshes were chosen based on our benchmark studies, where we checked the convergence of the band gap with respect to the k-point mesh size (Supplementary Fig. S6). Overall, parameters listed above guarantee all band gaps are converged within 0.01 eV. Since our experimental measurements only covered 8 different pressures, we linearly interpolated and extrapolated the crystal structure at 1, 1.5, 1.75, 2, 4, 4.5 and 5 GPa using the measured crystal structure for both low pressure and high pressure phases, in order to increase the coverage of the electronic band

structure computation. We note that the DFT calculations for pressures above 3.5 GPa assume no further phase transitions from the P2₁/c phase and are hence speculative, although a potential P2₁/m phase has been proposed in this pressure range². To compute the bandgap at various pressures, we used experimentally determined P–V curve to estimate volumes at selected pressures. Experimental structure and lattice parameters were scaled according to the estimated volume before relaxing the structure. Starting from these structures, we relaxed the atomic positions and the shape of the simulation cell while keeping the volume fixed²². The justification for this optimization procedure is provided in the Supplementary Note 1 and Figure S7.

Data availability

High pressure SXD crystallographic data for the structures reported in this article have been deposited at the Cambridge Crystallographic Data Centre. The specific deposition numbers are 2349102 (1 bar), 2349100 (0.27 GPa), 2349101 (0.63 GPa), 2349103 (1.30 GPa), 2349104 (2.08 GPa), 2349107 (2.47 GPa), 2349105 (3.50 GPa), 2349106 (2.98 GPa, decompression), and 2361519 (decompression, quenched to 1 bar). Copies of the data can be obtained free of charge at <https://www.ccdc.cam.ac.uk/structures/>. Data are also available in Supplementary Data 1.

Received: 26 April 2024; Accepted: 30 July 2024;

Published online: 08 August 2024

References

- Ullah, S. et al. All-inorganic CsPbBr₃ perovskite: a promising choice for photovoltaics. *Mater. Adv.* **2**, 646–683 (2021).
- Gong, J. B. et al. Pressure-induced indirect-direct bandgap transition of CsPbBr₃ single crystal and its effect on photoluminescence quantum yield. *Adv. Sci.* **9**, e2201554 (2022).
- Clinckemalie, L. et al. Challenges and opportunities for CsPbBr₃ perovskites in low- and high-energy radiation detection. *ACS Energy Lett.* **6**, 1290–1314 (2021).
- He, Y. H. et al. High spectral resolution of gamma-rays at room temperature by perovskite CsPbBr₃ single crystals. *Nat. Commun.* **9**, 1609 (2018).
- Li, X. et al. CsPbX₃ quantum dots for lighting and displays: room-temperature synthesis, photoluminescence superiorities, underlying origins and white light-emitting diodes. *Adv. Funct. Mater.* **26**, 2435–2445 (2016).
- Liu, P. et al. Air-stable high-PLQY cesium lead halide perovskites for laser-patterned displays. *J. Mater. Chem. C* **11**, 2282–2290 (2023).
- Ben Sadok, R., Muñoz, A., Rodríguez-Hernández, P., Djani, H. & Hammoutène, D. Pressure-driven ferroelectric phase transition for the Pnma-CsPbBr₃: mechanical and dynamical stability study. *J. Solid State Chem.* **314**, <https://doi.org/10.1016/j.jssc.2022.123402> (2022).
- Zhang, L., Zeng, Q. X. & Wang, K. Pressure-induced structural and optical properties of inorganic halide perovskite CsPbBr₃. *J. Phys. Chem. Lett.* **8**, 3752–3758 (2017).
- Zhang, D. Z. et al. Recent developments on high-pressure single-crystal X-ray diffraction at the Partnership for eXtreme Xtallography (PX2) program. *Phys Chem Miner* **49**, <https://doi.org/10.1007/s00269-022-01197-3> (2022).
- Cai, W. Z. et al. Pressure-induced ferroelectric-like transition creates a polar metal in defect antiperovskites Hg₃Te₂X₂ (X = Cl, Br). *Nat. Commun.* **12**, 1509 (2021).
- Guo, S. et al. Enhanced photocurrent of all-inorganic two-dimensional perovskite Cs₂PbI₂Cl₂ via pressure-regulated excitonic features. *J. Am. Chem. Soc.* **143**, 2545–2551 (2021).
- Kong, L. P. et al. Simultaneous band-gap narrowing and carrier-lifetime prolongation of organic-inorganic trihalide perovskites. *Proc. Natl Acad. Sci. USA* **113**, 8910–8915 (2016).

13. Lü, X. J. et al. Regulating off-centering distortion maximizes photoluminescence in halide perovskites. *Natl Sci. Rev.* **8**, nwa288 (2021).
14. Mao, Y. H. et al. Pressure-modulated anomalous organic-inorganic interactions enhance structural distortion and second-harmonic generation in MHyPbBr₃ perovskite. *J. Am. Chem. Soc.* **145**, 23842–23848 (2023).
15. Dove, M. T. Introduction to the theory of displacive phase transitions. *Nato Adv. Sci. I C.-Mat.* **543**, 427–450 (1999).
16. Christian, J. W., Olson, G. B. & Cohen, M. Classification of displacive transformations: what is a martensitic transformation? *J. Phys. IV* **5**, 3–10 (1995).
17. Gay, J. P. et al. Deformation of NaCoF₃ perovskite and post-perovskite up to 30 GPa and 1013 K: implications for plastic deformation and transformation mechanism. *Eur. J. Miner.* **33**, 591–603 (2021).
18. Wang, Y. J. et al. Spectroscopic properties and martensitic phase transition of Y₄Al₂O₉:Ce single crystals under high pressure. *Acta Mater.* **165**, 346–361 (2019).
19. Noculak, A. et al. Pressure-induced perovskite-to-non-perovskite phase transition in CsPbBr₃. *Helv. Chim. Acta* **104**, <https://doi.org/10.1002/hlca.202000222> (2021).
20. Gao, X. J. et al. Pressure effects on optoelectronic properties of CsPbBr₃ nanocrystals. *J. Phys. Chem. C* **124**, 11239–11247 (2020).
21. Yesudhas, S. et al. Pressure-induced phase changes in cesium lead bromide perovskite nanocrystals with and without Ruddlesden-Popper faults. *Chem. Mater.* **32**, 785–794 (2020).
22. Chen, Z., Teng, G. & Wei, S.-H. Origin of the nonmonotonic pressure dependence of the band gap in the orthorhombic perovskite CsPbBr₃. *J. Phys. Chem. Lett.* **15**, 1652–1657 (2024).
23. Szafranski, M. & Katrusiak, A. Photovoltaic hybrid perovskites under pressure. *J. Phys. Chem. Lett.* **8**, 2496–2506 (2017).
24. Zhang, R. et al. Effects of nonhydrostatic stress on structural and optoelectronic properties of methylammonium lead bromide perovskite. *J. Phys. Chem. Lett.* **8**, 3457–3465 (2017).
25. Klotz, S., Chervin, J. C., Munsch, P. & Le Marchand, G. Hydrostatic limits of 11 pressure transmitting media. *J. Phys. D Appl. Phys.* **42**, <https://doi.org/10.1088/0022-3727/42/7/075413> (2009).
26. Guennou, M., Bouvier, P., Haumont, R., Garbarino, G. & Kreisel, J. High-pressure phase transitions in BiFeO₃: hydrostatic versus non-hydrostatic conditions. *Phase Transit* **84**, 474–482 (2011).
27. Zhang, D. Z. et al. High pressure single crystal diffraction at PX2. *Jove-J. Vis. Exp.*, <https://doi.org/10.3791/54660> (2017).
28. Rivers, M. et al. The COMPRES/GSECARS gas-loading system for diamond anvil cells at the Advanced Photon Source. *High. Press. Res.* **28**, 273–292 (2008).
29. Shen, G. Y. et al. Toward an international practical pressure scale: A proposal for an IPPS ruby gauge (IPPS-Ruby2020). *High. Press. Res.* **40**, 299–314 (2020).
30. Sheldrick, G. M. Crystal structure refinement with SHELXL. *Acta Crystallogr C* **71**, 3–8 (2015).
31. Dolomanov, O. V., Bourhis, L. J., Gildea, R. J., Howard, J. A. K. & Puschmann, H. OLEX2: a complete structure solution, refinement and analysis program. *J. Appl. Crystallogr* **42**, 339–341 (2009).
32. Giannozzi, P. et al. QUANTUM ESPRESSO: a modular and open-source software project for quantum simulations of materials. *J. Phys.-Condens Mat.* **21**, 395502 (2009).
33. Boerner, T. J., Deems, S., Furlani, T. R., Knuth, S. L. & Towns, J. in *Practice and Experience in Advanced Research Computing* 173–176 (Association for Computing Machinery, Portland, OR, USA, 2023).
34. Perdew, J. P., Burke, K. & Ernzerhof, M. Generalized gradient approximation made simple. *Phys. Rev. Lett.* **77**, 3865–3868 (1996).
35. Kresse, G. & Joubert, D. From ultrasoft pseudopotentials to the projector augmented-wave method. *Phys. Rev. B* **59**, 1758–1775 (1999).
36. Wang, X. Y. et al. Pressure effects on the structures and electronic properties of halide perovskite CsPbX₃ (X = I, Br, Cl). *Phys. Chem. Chem. Phys.* **23**, 3479–3484 (2021).
37. Huang, Y., Wang, L. R., Ma, Z. & Wang, F. Pressure-Induced Band Structure Evolution of Halide Perovskites: A First-Principles Atomic and Electronic Structure Study. *J. Phys. Chem. C* **123**, 739–745 (2019).
38. Maphoto, R. I., Morukuladi, M. T., Malatji, K. T., Masedi, M. C. & Ngoepe, P. E. First-principle study of CsPbBr₃ and CsPbI₃ perovskite solar cells. *Ecs J Solid State Sci.* **11**, <https://doi.org/10.1149/2162-8777/ac5eb6> (2022).
39. Perdew, J. P. & Levy, M. Physical content of the exact Kohn-Sham orbital energies: band gaps and derivative discontinuities. *Phys. Rev. Lett.* **51**, 1884–1887 (1983).

Acknowledgements

This work was performed at GeoSoilEnviroCARS (Sector 13), Advanced Photon Source (APS), and Argonne National Laboratory. GeoSoilEnviroCARS is supported by the National Science Foundation–Earth Sciences (EAR-1634415) and Department of Energy–Geosciences (DE-FG02-94ER14466). Part of this study is supported by COMPRES under NSF Cooperative Agreement EAR-1661511. Use of the Advanced Photon Source was supported by the U.S. Department of Energy, Office of Science, Office of Basic Energy Sciences, under Contract No. DE-CO2-6CH11357. Part of this research is supported by NSF CSEDI EAR-2246686 (DZ) and EAR-2246687 (MC). We gratefully acknowledge the computing resources provided on Bebop, a high-performance computing cluster operated by the Laboratory Computing Resource Center at Argonne National Laboratory. This work also used Anvil at Purdue University through allocation CHE220008 from the Advanced Cyberinfrastructure Coordination Ecosystem: Services & Support (ACCESS) program, which is supported by National Science Foundation grants #2138259, #2138286, #2138307, #2137603, and #2138296. The synthesis and crystal growth work were supported by the U.S. Department of Energy, Office of Science, Basic Energy Sciences, Materials Sciences and Engineering Division.

Author contributions

Conceptualization: D.Z., M.C. Sample synthesis: D.Y.C., M.G.K. High pressure X-ray diffraction experiments and analysis: D.Z., J.X. DFT calculations and analysis: D.Z., S.M., N.S., M.C. Visualization: D.Z., S.M. Investigation: D.Z., S.M., M.C. Writing, review & editing: D.Z., S.M., D.Y.C., J.X., N.S., M.G.K., M.C.

Competing interests

The authors declare no competing interests.

Additional information

Supplementary information The online version contains supplementary material available at <https://doi.org/10.1038/s42004-024-01265-5>.

Correspondence and requests for materials should be addressed to Dongzhou Zhang or Ming Chen.

Peer review information *Communications Chemistry* thanks the anonymous reviewers for their contribution to the peer review of this work.

Reprints and permissions information is available at <http://www.nature.com/reprints>

Publisher's note Springer Nature remains neutral with regard to jurisdictional claims in published maps and institutional affiliations.

Open Access This article is licensed under a Creative Commons Attribution-NonCommercial-NoDerivatives 4.0 International License, which permits any non-commercial use, sharing, distribution and reproduction in any medium or format, as long as you give appropriate credit to the original author(s) and the source, provide a link to the Creative Commons licence, and indicate if you modified the licensed material. You do not have permission under this licence to share adapted material derived from this article or parts of it. The images or other third party material in this article are included in the article's Creative Commons licence, unless indicated otherwise in a credit line to the material. If material is not included in the article's Creative Commons licence and your intended use is not permitted by statutory regulation or exceeds the permitted use, you will need to obtain permission directly from the copyright holder. To view a copy of this licence, visit <http://creativecommons.org/licenses/by-nc-nd/4.0/>.

© The Author(s) 2024